P-type ZnO by Sb doping for PN-junction photodetectors

J. L. Liu, F. X. Xiu, L. J. Mandalapu, Z. Yang

Quantum Structures Laboratory, Department of Electrical Engineering,
University of California, Riverside, CA 92521

ABSTRACT

Sb-doped p-type ZnO films were grown on n-Si (100) by electron cyclotron resonance (ECR)-assisted molecular-beam epitaxy (MBE). Room temperature Hall effect measurements reveal that a heavily Sb-doped ZnO sample exhibits a low resistivity of 0.2 Ω cm, high hole concentration of 1.7×10^{18} cm^{-3}, and high mobility of 20.0 cm^2/V s. Low-temperature photoluminescence (PL) measurements show an Sb-associated acceptor-bound exciton (AºX) emission exists at 3.358 eV at 8.5 K. The acceptor energy level of the Sb dopant is estimated to be 0.14 eV above the valence band. Based on these electrical and optical properties, p-n hetero- and homojunction photodetectors employing Sb-doped p-type ZnO films were designed and fabricated. The heterojunction photodiode consists of Sb-doped p-type ZnO grown on n-Si (100) substrate. An Sb-doped p-type ZnO layer with an n-type Ga-doped ZnO layer was grown on a p-Si (111) substrate to form the homojunction. Current-Voltage (I-V) characterizations reveal rectifying characteristics. Good photoresponse to UV light has been demonstrated for both hetero and homojunction photodetectors.

Keywords: ZnO, Sb doping, photoluminescence, Hall effect, homojunction, heterojunction, photodetector

1. INTRODUCTION

To realize efficient ZnO-based optoelectronic and spintronic devices, both p-type and n-type ZnO are necessary. However, the fabrication of p-type ZnO is difficult due to the self-compensating effect from native defects (V_o and Zn_i) and H incorporation.[1] In addition, the low solubility and the deep acceptor levels of the dopants may yield low carrier concentrations, making p-ZnO even harder to fabricate. Although many approaches, such as group-V element doping (N,[2] P,[3] and As[4]) and III-V co-doping[5] have been extensively attempted to dope ZnO, the resultant p-type conduction is still not reproducible. For this reason, many devices that use just n-type ZnO have been reported.[6-12] For specific example, heterojunctions based on n-type ZnO and different p-type materials, such as GaN,[9] SiC,[10] Si,[11] and AlGaN,[12] were studied. But, only limited heterojunction diodes using p-type ZnO[13-15] and homojunctions[15-18] were reported. In this paper, we first report the growth and characterizations of reliable p-type ZnO by Sb doping, then we discuss the fabrication and characterization of Sb-doped p-ZnO/n-Si heterojunction photodiodes, as well as Sb-doped p-type ZnO and Ga-doped n-type ZnO based homojunction photodiodes.

2. EXPERIMENT

To characterize electrical and optical properties of Sb-doped ZnO films, high-resistive Si (100) (20–30 Ω cm) was used as the substrate. Prior to growth, they were cleaned by a modified Piranha-HF method. First, the substrate was dipped in Piranha solution (H_2O_2:H_2SO_4 = 3:5) for 1 min and then, in aqueous HF solution (HF:H_2O = 1:10) for 1 min to hydrogenate the substrate surface. This procedure was repeated three times. During the film growth, elemental Zn (5N) and Sb (5N) sources were provided by conventional low-temperature effusion cells. Oxygen (5N) plasma was generated by an ECR source. Four steps were introduced in order to grow a single layer of Sb-doped ZnO with a thickness of approximately 200 nm. In step I, the Si substrate was thermally cleaned at 650 ˚C for 10 min to disassociate hydrogen bonds, leaving a fresh Si surface for subsequent growth. In step II, a thin Zn metallic layer was deposited on the Si substrate for 10 s to minimize the formation of SiO_2 prior to or during growth. In step III, an Sb-doped ZnO film was grown at 550 ˚C with an oxygen flow rate

of 25 sccm and a growth pressure of 1.3×10^{-3} Torr, which corresponds to an oxygen-rich condition. This growth condition is believed to effectively depress the formation of Zn_i and V_o vacancies, and therefore minimizing the background electron concentration. In step IV, post-annealing under vacuum was performed to thermally activate Sb dopants. The heterojunction photodiode sample under discussion was annealed at 650 ˚C after growth. In case of the homojunction sample, an Sb-doped ZnO layer was grown on p-Si (111) substrate of resistivity 10–40 Ω cm at 550 ˚C, followed by post-annealing at 800 ˚C. A Ga-doped ZnO layer was subsequently grown on top of this layer to form the p-n homojunction. The thickness of both the Ga-doped and Sb-doped ZnO layers are 500 nm.

Hall effect and electrical resistivity measurements were conducted with a Physical Property Measurement System by Quantum Design. All Sb-doped ZnO films were prepared in a van der Pauw configuration. Low-temperature PL measurements were carried out using a 5 mW He-Cd laser with an excitation wavelength of 325 nm. The laser beam was impinged on the sample surface with an angle of approximately 60˚. The excited PL emission was measured with an Oriel monochromator, aligned normal to the sample surface.

Conventional photolithography was used to fabricate devices from the as-grown samples. The heterojunction diode was fabricated by depositing top metal contacts of size 120 μm × 180 μm and a backside contact, while the homojunction sample was fabricated by defining 250 μm × 250 μm mesas. A diluted solution of 1: 1: 160 of acetic acid: phosphoric acid: water was used as the etchant of ZnO. Al/Ti metal was deposited by e-beam evaporation and standard lift off was used to form the contact electrodes of the device. Following this, annealing at 550 ˚C for 30 s was performed to eliminate barriers and make the contacts Ohmic. After the fabrication, I-V measurements were carried out using an Agilent 4155C semiconductor parameter analyzer and a Signatone probe station. The samples were packaged onto TO5 cans before performing photocurrent (PC) measurements using a home-built system.

3. RESULTS AND DISCUSSION

To study the electrical properties of the Sb-doped ZnO films, Hall effect and resistivity measurements were performed as a function of temperature. Figure 1 shows the temperature-dependent hole concentration (p_H) for a typical heavily doped ZnO film with an Sb dopant cell temperature of 350 ˚C. The inset of Fig. 1 shows the Hall resistance R_{Hall} as a function of magnetic field at 300 K. The positive slope, meaning the positive Hall coefficient, shows p-type conduction. The acceptor activation energy (E_A) can be extracted by fitting the experimental data with the equation $p \propto T^{3/2} \exp(-E_A / k_B T)$.[16] At temperatures below ~80 K, the hole concentration decreases dramatically resulting from the tremendous freeze-out of carriers. In this temperature region, the acceptor activation energy is obtained as 82 meV, which is much lower than the value obtained from PL spectra (140 meV as discussed later). This phenomenon is believed to arise from the widely-observed screening effect.[19] At temperatures above ~80 K, a half value of activation energy (41 meV) is obtained, similar to the senario of p-type Si.[20] At 80 K, the kink temperature, the concentration of compensating donor impurities can be identified and estimated as $~7.0 \times 10^{17}$ cm^{-3}.

Figure 2 shows the temperature dependence of Hall mobility μ_H. Values of 20.0 cm^2/V s and 1900.0 cm^2/V s were obtained at 300 K and 40 K, respectively. In this temperature range, μ_H is found to be proportional to $T^{-3/2}$ indicating that acoustic phonon scattering dominates at these temperatures. The inset of Fig. 2 shows the electrical resistivity as a function of temperature. A low value of 0.2 Ω cm was obtained at room temperature, which is comparable to a reported value of 0.4 Ω cm for As-doped ZnO.[21] Consistent with the observed temperature variation of the carrier concentration, the resistivity increases with temperature above 80 K. It is known that resistivity depends inversely on the hole concentration and the scattering time, which are both temperature dependent. At low temperatures, the number of carriers changes much more rapidly than the scattering time, and this dominates the temperature dependence of the resistivity. As the temperature is increased above 80 K, the temperature variation in the number of carriers is much less dramatic, as indicated in the Fig. 1, and the decreasing scattering time overcomes the increasing number of carriers, resulting in an increasing resistivity with temperature.

The Sb-doped *p*-type ZnO layer in the heterojunction sample was found to have a hole concentration, mobility, and resistivity of 1.0×10^{18} cm^{-3}, 22.4 cm^2/V s, and 0.27 Ω cm, respectively, while the layer in homojunction sample has a hole concentration, mobility, and resistivity of 1.0×10^{16} cm^{-3}, 10.0 cm^2/V s, and 6.0 Ω cm, respectively at room temperature. The electron concentration, mobility, and resistivity of the Ga-doped ZnO layer are 1.0×10^{18} cm^{-3}, 6.0 cm^2/V s, 0.9 Ω cm, respectively. Since the lattice mismatch between ZnO and Si (111) is smaller than that between ZnO and Si (100), the ZnO thin films grown on Si (111) substrate are expected to have a better crystalline quality than the ZnO films grown on Si (100) substrate. Hence, the electrical properties from the Sb-doped ZnO layers on Si (111) and Si (100) are different.
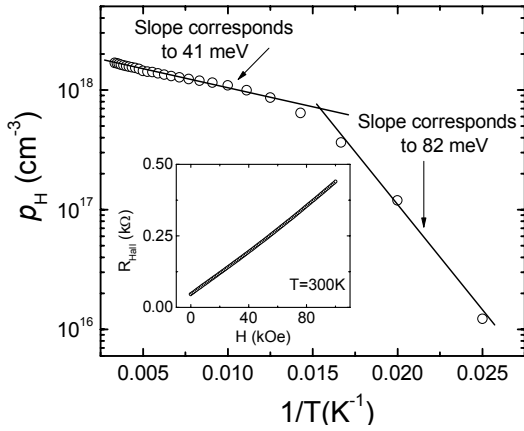

Figure 1. Temperature dependence of hole concentration in an Sb-doped *p*-type ZnO film. Hall resistance as a function of applied magnetic field is shown in the inset at *T* = 300 K.
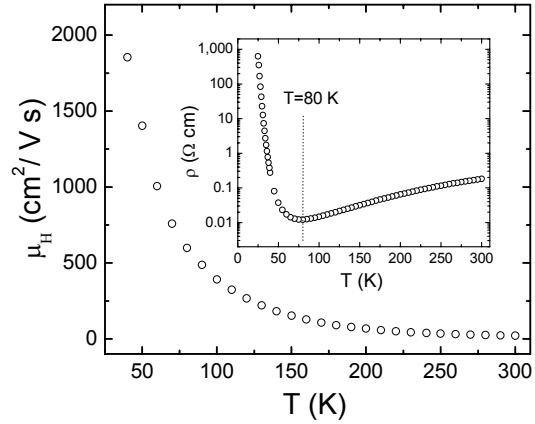

Figure 2. Temperature dependence of the Hall mobility for an Sb-doped ZnO film. The inset shows the temperature dependence of electrical resistivity.

To obtain the acceptor binding energy of Sb-doped ZnO films, the temperature-dependent PL measurements were performed from 8.5 to 300 K, as shown in Fig. 3. At the temperature of 8.5 K, a strong A°X was clearly observed at 3.358 eV, which is a typical feature of *p*-type ZnO.[21] The other Sb-associated emissions show up at 3.296, 3.222, and 3.050 eV. With an increase of the temperature from 8.5 to 100 K, emissions at 3.296 and 3.222 eV show slight blue-shifts, which are typical characteristics of free electron to acceptor (FA) and donor-acceptor pair (DAP) transitions.[22] In addition, over the whole temperature range, 3.222 eV emission-line gradually merges into 3.296 eV emission-line, showing the feature of the thermal ionization of donors.[23] Therefore, these two emissions at 3.296 and 3.222 eV were identified as FA and DAP transitions, respectively.[24,25] The emission around 3.050 eV (at 8.5 K) is believed to be associated with Zn vacancies.[26] Thus, a red-shift with the increase of temperature in Fig. 3 indicates that the deep acceptor levels associated with Zn vacancies have formed a band.[24] The appearance of the FA emission makes it possible to calculate the acceptor binding energy (E_A) at 8.5 K with[22]
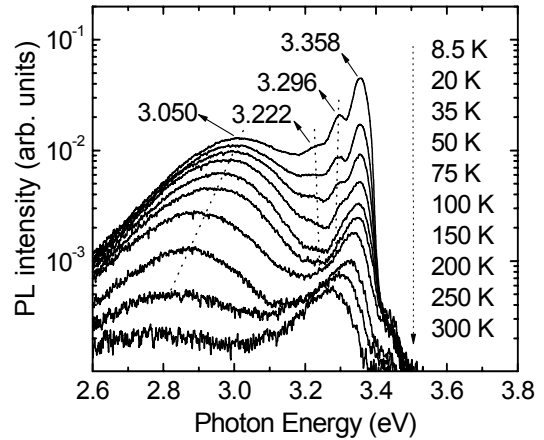

Figure 3. PL spectra measured at several temperatures over the range from 8.5 to 300 K for a heavily Sb-doped ZnO film with an Sb dopant cell temperature of 350 °C.

$$E_A = E_{gap} - E_{FA} + k_B T / 2 \qquad (1)$$

where E_{FA} is the temperature-dependent transitions, and E_{FA}=3.296 eV at 8.5 K . With an intrinsic band gap of E_{gap} = 3.437 eV at 8.5 K, the value of E_A is calculated to be 0.14 eV. These experimental results shed new light on the Sb doping mechanism. Recently, Limpijumnong et al.[27] proposed a model for large-size-mismatch group-V dopants in ZnO. Specifically, it is predicted that Sb would not occupy the O site as is widely perceived, but rather the Zn site, and simultaneously induce two Zn vacancies to form a complex (Sb_{Zn}–$2V_{Zn}$). This complex has low acceptor-ionization energy of 160 meV, therefore serving as a shallow acceptor to provide p-type conductivity. The fact that shallow acceptor levels of 140 meV were resolved from our PL analysis is an indication of the formation of defect complex (Sb_{Zn}–$2V_{Zn}$). Nevertheless, the appearance of Zn vacancy-related emission at 3.050 eV in the heavily Sb-doped ZnO film suggests the co-existence of defect complex (Sb_{Zn}–$2V_{Zn}$) and isolated defect V_{Zn}.

Figure 4 shows the I-V characteristics of the heterojunction diode plotted on a semi-log scale. Clear rectifying curves for the device were observed but the rectification has an inverse trend of a p-n junction similar to that of a p-type Schottky diode. The turn-on voltage of the diode is around -2.4 V. The left inset in Fig. 4 gives the I-V characteristics of annealed top and back contacts on the ZnO and Si layers, respectively, on a log-log scale. The linear characteristics confirm Ohmic behavior from the contacts. The inset on right shows the energy band diagram of the heterojunction at equilibrium. The energy band diagram was constructed based on Anderson's model,[16,17] by using the electron affinity of Si (χ_{Si}=4.05 eV)[17] and ZnO(χ_{ZnO}=4.35 eV).[18] A small conduction band offset of 0.3 eV and a large valence band offset of 2.45 eV exists in the band structure. At the equilibrium, a quantum well for holes is formed on the Si side at the interface. The valence band offset acts as a barrier for the conduction of holes from p-ZnO to n-Si, thus limiting the conducted current. In this structure, the smaller-bandgap material, Si is similar to the metal and the valence band offset is equivalent to a Schottky barrier, in a p-type diode, which is consistent with the observed I-V characteristics. The forward I-V characteristics follow the relation for the thermionic emission over a barrier: $J_F = A^* T^2 \exp(-e\Phi_b/kT) \exp(eV/nkT)$, where, J_F is the current density, A^* is the Richardson's constant for p-ZnO, T the absolute temperature, e the electronic charge, Φ_b the barrier height, k Boltzmann's constant, n the ideality factor, and V the applied voltage. However, the ideality factor cannot be determined here because the precise area of the junction is not known, as mesas were not defined in this experiment for the heterojunction diodes. The dark current is large, about 1.76×10^{-4} A at 5 V due to the imperfect ZnO/Si interface and poor hetero-epitaxial ZnO film quality. The diode did not show any signs of breakdown until 40 V, although there is an increase in the leakage current.
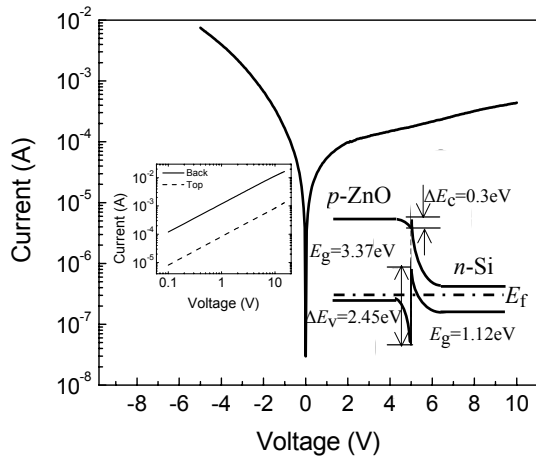

Figure 4. I-V characteristics of the heterojunction photodiode in dark. The inset on left shows the I-V curves obtained from the ohmic back and top contacts. The right inset gives the energy band diagram at equilibrium.
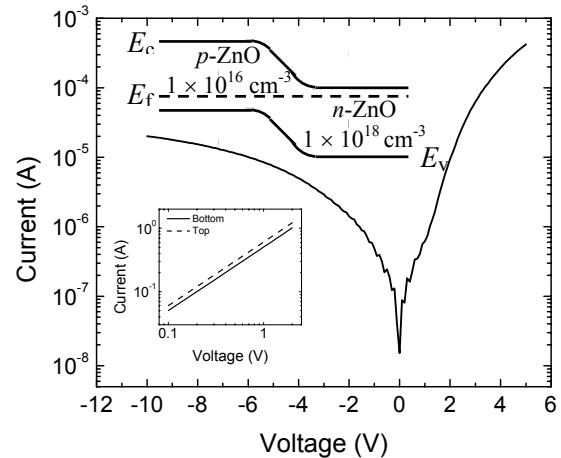

Figure 5. I-V characteristics of the homojunction diode in dark. The top inset gives the energy band diagram at equilibrium. The lower inset gives the I-V characteristics of the top and bottom ohmic contacts.

I-V characteristics of the homojunction diode in dark are shown in Fig. 5. Rectifying I-V curves show the existence of the p-n junction. The bottom inset gives the Ohmic I-V characteristics from contacts on Sb-doped and Ga-doped ZnO layer after

annealing. The band diagram of the junction at equilibrium is shown as the top inset of Fig. 5. The turn-on voltage of the homojunction diode is around 2 V. Based on the characterized doping concentrations of the *p*-type and *n*-type layers in this homojunction device, the built-in potential (turn-on voltage) of about 2 V is obtained if the intrinsic carrier concentration of 1×10^0 cm^{-3} is used, which is reasonable due to the wide bandgap of ZnO. The dark current density of the device is about 12 mA/cm^{-2} at –5 V again due to the poor crystalline quality of the ZnO films, which is in-turn due to the hetero-epitaxy between largely mismatched ZnO and Si.

To investigate the response of the device to specific wavelengths, PC measurements were carried out. Figure 6 gives the PC spectra at zero bias obtained from the heterojunction and homojunction photodetectors. Photoresponse from the devices begins around 260 nm in the UV region and extends into the visible region. The low penetration depth limits the response to the high-energy light. The response increases steadily reaching a peak around 350nm corresponding to the effective bandgap of ZnO. The wavelength, 366 nm at which a dip is seen in the response corresponds to the bandgap of ZnO (~3.38 eV). The response to UV light below 366 nm is attributed to the absorption in the ZnO layer as the high energy UV light (short wavelength) is absorbed by ZnO before it reaches the Si layer. Increase in the response starting from wavelengths beyond approximately 366 nm occurs due to the absorption in the Si layer. Once the energy of the incident photons is smaller than the bandgap of ZnO, ZnO becomes transparent to such light and the depletion region in Si starts the absorption in the heterojunction photodiode. In case of the homojunction diode, since the doping concentration of the *p*-type ZnO layer is small, the depletion region on the *p*-side extends into the Si layer resulting in the photoresponse in visible region.
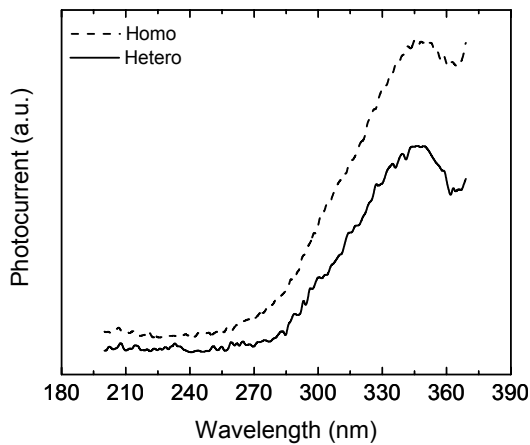

Figure 6. Photocurrent spectra obtained from heterojunction (solid) and homojunction (dotted) photodiodes. The curves are displaced for clarity.

4. CONCLUSION

In summary, *p*-type ZnO films were achieved with MBE by Sb doping. Electrical properties were investigated by the Hall effect and resistivity measurements. It is revealed that high carrier concentration of 1.7×10^{18} cm^{-3} and mobility of 20.0 cm^2/V s can be achieved by Sb doping. From low-temperature PL measurements, it is inferred that Sb has a low binding energy of 140 meV, which is consistent with theoretical calculation of 160 meV. The observation of isolated Zn vacancies in low-temperature PL further indicates the possible doping mechanism by forming Sb$_{Zn}$–2V$_{Zn}$ as the shallow acceptor. The *p-n* hetero- and homojunction photodetectors based on Sb-doped *p*-type ZnO were grown, fabricated and characterized. Rectifying *I-V* curves were observed from both the devices. The capabilities of these devices for photodetection were studied. PC spectra showed very good response in the UV region for both the hetero- and homojunction diodes. The demonstration of good performances from Sb-doped *p*-type ZnO/*n*-type Si heterojunction photodiodes and Ga-doped *n*-type ZnO/Sb-doped *p*-type ZnO homojunction photodiodes suggests that these devices are very promising for UV photodetector applications.

5. ACKNOWLEDGEMENTS

6. REFERENCES

[1]   C. G. Van de Walle, Phys. Rev. Lett. **85**, 1012 (2000).

[2]   D. C. Look, D. C. Reynolds, C. W. Litton, R. L. Jones, D. B. Eason, and G. Cantwell, Appl. Phys. Lett. **81**, 1830 (2002).

[3]   K. K. Kim, H. S. Kim, D. K. Hwang, J. H. Lim, and S. J. Park, Appl. Phys. Lett. **83**, 63 (2003).

[4]   Y. R. Ryu, T. S. Lee, and H. W. White, Appl. Phys. Lett. **83**, 87 (2003).

[5]   J. G. Lu, Z. Z. Ye, F. Zhuge, Y. J. Zeng, B. H. Zhao, and L. P. Zhu, Appl. Phys. Lett. **85**, 3134 (2004).

[6]   Y. Polyakov, N. B. Smirnov, E. A. Kozhukhova, V. I. Vdovin, K. Ip, Y. W. Heo, D. P. Norton, and S. J. Pearton, J. Vac. Sci. Technol. A **21**, 1603 (2003).

[7]   Y. Liu, C. R. Gorla, S. Liang, N. Emanetogulu, Y. Lu, H. Shen, and M. Wraback, J. Electron. Mater. **29**, 69 (2000).

[8]   Y. H. Heo, Y. W. Kwon, Y. Li, S. J. Pearton, and D. P. Norton, Appl. Phys. Lett. **84**, 3474 (2004).

[9]   Y. I. Alivov, J. E. V. Nostrand, D. C. Look, M. V. Chukichev, and B. M. Ataev, Appl. Phys. Lett. **83**, 2943 (2003).

[10] Y. I. Alivov, Ü. Özgür, S. Doğan, D. Johnstone,V. Avrutin, N.Onojima, C. Liu, J. Xie, Q. Fan, and H. Morkoç, Appl. Phys. Lett. **86**, 241108 (2005).

[11] S. Jeong, J. H. Kim, and S. Im, Appl. Phys. Lett. **83**, 2946 (2003).

[12] Y. I. Alivov, E. V. Kalinina, A. E. Cherenkov, D. C. Look, B. M. Ataev, A. K. Omaev, M. V. Chukichev, and D. M. Bagnall, Appl. Phys. Lett. **83**, 4719 (2003).

[13] D. Wang, Y. C. Liu, R. Mu, J. Y. Zhang, Y. M. Lu, D. Z. Shen, and X. W. Fan, J. Phys.: Condens. Matter **16**, 4635 (2004).

[14] D. K. Hwang, S. H. Kang, J. H. Lim, E. J. Yang, J. Y. Oh, J. H. Yang, and S. J. Park, Appl. Phys. Lett. **86**, 222101 (2005).

[15] F. Zhuge, L. P. Zhu, Z. Z. Ye, D. W. Ma, J. G. Lu, J. Y. Huang, F. Z. Wang, Z. G. Ji, and S. B. Zhang, Appl. Phys. Lett. **87**, 092103 (2005).

[16] A. Tsukazaki. Ohtomo, T. Onuma, M. Ohtani, T. Makino, M. Sumiya, K. Ohtani, S. F. Chichibu, S. Fuke, Y. Segawa, H. Ohno, H. Koinuma, and M. Kawasaki, Nat. Mater. **4**, 42 (2005).

[17] T. Aoki, Y. Hatanaka, and D. C. Look, Appl. Phys. Lett. **76**, 3257 (2000).

[18] Y. R. Ryu, W. J. Kim, and H. W. White, J. Cryst. Growth **219**, 419 (2000).

[19] D. C. Look, Semicond. Sci. Technol. **20**, S55 (2005).

[20] K. Seeger, *Semiconductor Physics*, 3rd ed (Springer, Berlin, 1985).

[21] D. C. Look, G. M. Renlund, R. H. Burgener II, and J. R. Sizelove, Appl. Phys. Lett. **85**, 5269 (2004).

[22] K. Tamura, T. Makino, A. Tsukazaki, M. Sumiya, S. Fuke, T. Furumochi, M. Lippmaa, C. H. Chia, Y. Segawa, H.

Koinuma, and M. Kawasaki, Solid State Commun. **127**, 265 (2003).

[23] B. K. Meyer, H. Alves, D. M. Hofmann, W. Kriegseis, D. Forster, F. Bertram, J. Christen, A. Hoffmann, M. Straßburg, M. Dworzak, U. Haboeck, and A. V. Rodina, Phys. Status Solidi B **241**, 231 (2004).

[24] F. X. Xiu, Z. Yang, L. J. Mandalapu, D. T. Zhao, and J. L. Liu, Appl. Phys. Lett. **87**, 252102 (2005).

[25] F. X. Xiu, Z. Yang, L. J. Mandalapu, D. T. Zhao, J. L. Liu, and W. P. Beyermann, Appl. Phys. Lett. **87**, 152101 (2005).

[26] B. X. Lin, Z. X. Fu, and Y. B. Jia, Appl. Phys. Lett. **79**, 943 (2001).

[27] S. Limpijumnong, S. B. Zhang, S. H. Wei, and C. H. Park, Phys. Rev. Lett. **92**, 155504 (2004).